

# Non-contact optical magnetic field sensor based on metamaterial nanomechanics F

Cite as: APL Photonics 7, 036101 (2022); <https://doi.org/10.1063/5.0081849>

Submitted: 10 December 2021 • Accepted: 06 February 2022 • Accepted Manuscript Online: 07 February 2022 • Published Online: 01 March 2022

 Guoqiang Lan,  Jun-Yu Ou,  Dimitrios Papas, et al.

## COLLECTIONS

 This paper was selected as Featured



View Online



Export Citation



CrossMark

## ARTICLES YOU MAY BE INTERESTED IN

[Distributed deep learning training using silicon photonic switched architectures](#)

APL Photonics 7, 030901 (2022); <https://doi.org/10.1063/5.0070711>

[A perspective on twisted light from on-chip devices](#)

APL Photonics 6, 110901 (2021); <https://doi.org/10.1063/5.0060736>

[Optomechanical metamaterial nanobolometer](#)

APL Photonics 6, 126110 (2021); <https://doi.org/10.1063/5.0073583>

SUBMIT TODAY!

## AVS Quantum Science

# SPECIAL TOPIC: Quantum Networks: Past, Present and Future

Co-Published by



# Non-contact optical magnetic field sensor based on metamaterial nanomechanics

Cite as: APL Photon. 7, 036101 (2022); doi: 10.1063/5.0081849  
Submitted: 10 December 2021 • Accepted: 6 February 2022 •  
Published Online: 1 March 2022



Guoqiang Lan,<sup>1,2</sup>  Jun-Yu Ou,<sup>1,a)</sup>  Dimitrios Papas,<sup>1</sup>  Nikolay I. Zheludev,<sup>1,3</sup>  and Eric Plum<sup>1,a)</sup> 

## AFFILIATIONS

<sup>1</sup> Optoelectronics Research Centre and Centre for Photonic Metamaterials, University of Southampton, Highfield, Southampton SO17 1BJ, United Kingdom

<sup>2</sup> School of Electronic Engineering, Heilongjiang University, No. 74 Xuefu Road, Harbin 150080, China

<sup>3</sup> Centre for Disruptive Photonic Technologies, SPMS, TPI, Nanyang Technological University, Singapore 637371, Singapore

<sup>a)</sup> Authors to whom correspondence should be addressed: [bruce.ou@soton.ac.uk](mailto:bruce.ou@soton.ac.uk) and [erp@orc.soton.ac.uk](mailto:erp@orc.soton.ac.uk)

## ABSTRACT

We demonstrate a non-contact optical magnetic field sensor that is based on actuation of a metamaterial-microcavity by the magnetic Lorentz force. Magnetic field is transduced to a change of the sensor's reflectivity. The microscale proof-of-concept metamaterial magnetometer can be read from a distance and offers 60  $\mu\text{m}$  spatial, about 10  $\mu\text{s}$  temporal, and sub-microtesla magnetic field resolution.

© 2022 Author(s). All article content, except where otherwise noted, is licensed under a Creative Commons Attribution (CC BY) license (<http://creativecommons.org/licenses/by/4.0/>). <https://doi.org/10.1063/5.0081849>

## I. INTRODUCTION

While some plants<sup>1</sup> and animals<sup>2</sup> evolved the ability to sense the magnetic field, manmade magnetite compasses<sup>3</sup> have been used for fortune-telling and geomancy in China at least since the Han dynasty more than 2000 years ago. At the present time, magnetic fields are used in electrical motors and generators, in data storage computer disks, to control nuclear fusion reactors and particle accelerators, in medical scanning techniques, and in many other applications. Detection of magnetic fields is important for finding minerals, navigation, reading data from magnetic disks, bank note security, and medical and brain function imaging.<sup>4–9</sup> Despite the development of a large range of magnetometers,<sup>4,10,11</sup> small magnetic field sensors combining high spatial and temporal resolution at room temperature with non-contact readout remained a challenge. Conventional magnetometers based on induction, fluxgates, magnetoimpedance, magnetoimpedance, nuclear magnetic resonance, and the Hall effect or SQUIDs rely on wired electrical readout and have resolution/temperature limitations. In contrast, optical sensors have the advantage that they can be read from a distance, enabling non-contact measurements and use in harsh environments. However, fiberized<sup>12,13</sup> and optical fiber magnetometers<sup>14–18</sup> (based on the Lorentz force,<sup>12</sup> Faraday effect,<sup>14,15</sup> magnetic fluids,<sup>16–18</sup> Fabry-Pérot cavities,<sup>17,18</sup> and vapor cells<sup>13</sup>) rely on the fiber connection for readout. Non-contact optical magnetic resonance detection based on nitrogen-vacancy centers in diamond can achieve

sub-micron spatial resolution and high sensitivity, but the simultaneous need for light, microwaves, and an external magnetic field prevents microscale integration.<sup>19,20</sup> Similarly, all-optical atomic magnetometers cannot be miniaturized to microscale dimensions,<sup>13,21</sup> and mm-scale micromachined magnetic field sensors relying on laser beam deflection for readout require large optical systems.<sup>22–24</sup> Reconfigurable photonic metamaterials<sup>25</sup> with optical properties controlled by electromagnetic forces provide an opportunity to develop small optical sensors that are read based on a change of the optical properties of the sensing element itself. Here, we report the proof-of-principle demonstration of an optical magnetic field sensor based on the Lorentz force actuation of a metamaterial microcavity. The magnetic field is transduced to a change of the structure's reflectivity, and the sensing characteristics may be engineered by the metamaterial design. Such sensors of microscale dimensions offer 10s of micrometer spatial, about 10  $\mu\text{s}$  temporal, and sub-microtesla magnetic field resolution as well as non-contact optical readout. Novel aspects of this work include the demonstration of a metamaterial magnetometer, use of metamaterial-microcavity actuation for sensing, and realization of a microscale Fabry-Pérot magnetic field sensor with non-contact readout.

This paper is organized as follows: Section II introduces the operating principle of the magnetic field sensor along with key mechanical and thermal design considerations. Section III reports

on the experimental proof-of-principle demonstration of a sensor device.

## II. CONCEPT AND THEORY

The sensor consists of a magnetically actuated microcavity formed by a static mirror and a metamaterial [Fig. 1(a)]. The

metamaterial is supported by a flexible beam actuator of nanoscale thickness and length  $L$ , which is displaced by the Lorentz force,  $F_L = LI \times B$ , acting on an electrical current  $I$  flowing along the beam in the presence of a magnetic field  $B$ . Such displacement changes the cavity length (referred to as gap  $g$ ) and, thus, the reflectivity of the device. The sensor's reflectivity is determined by multiple reflections of incident light within the cavity, which, depending on the cavity gap, may yield destructive or constructive interference on the

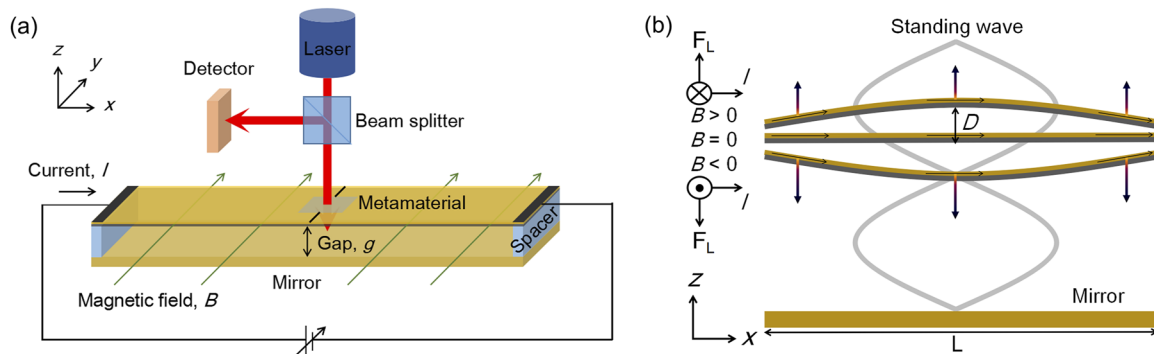


**FIG. 1.** Nanomechanical optical magnetic field sensing. (a) Schematic of the sensor consisting of a Fabry-Pérot microcavity formed by a static mirror and a metamaterial on an elastic beam of length  $L$  that carries a current  $I$ . (b) The Lorentz force  $F_L = LI \times B$  acting on the current in the presence of magnetic field  $B$  displaces the beam by a distance  $D$ , changing the cavity gap  $g$ . This causes a magnetic-field-dependent change in light absorption in the metamaterial, which can be read by detecting the intensity of reflected light.

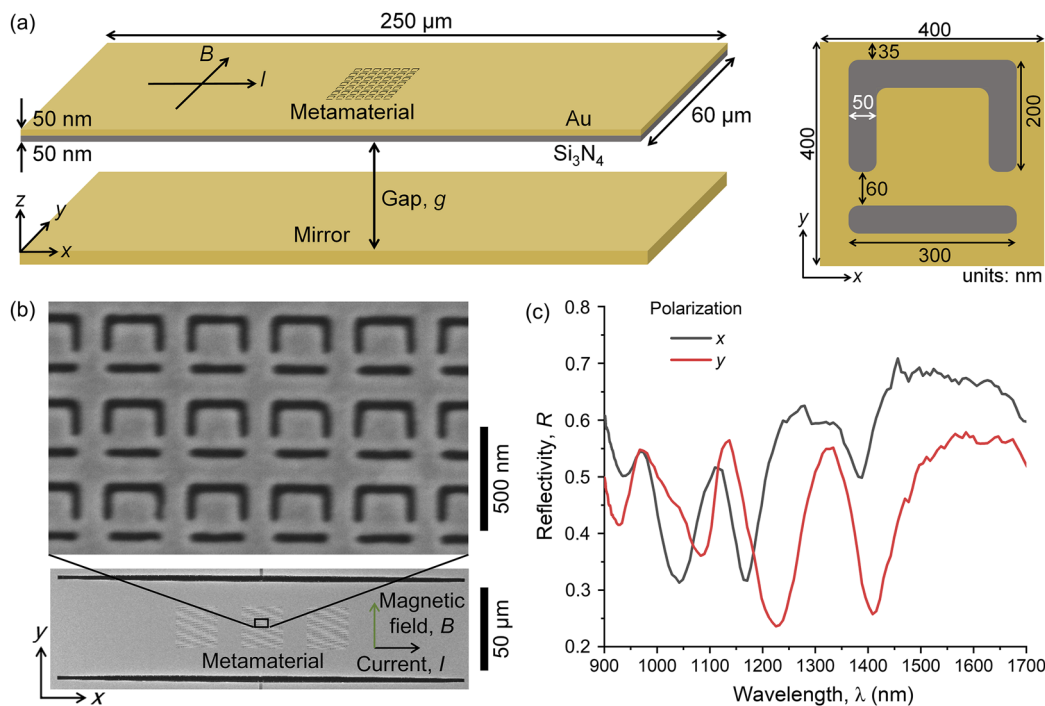


**FIG. 2.** The sensor and its optical properties. (a) Dimensions of the microcavity consisting of a static mirror and a metamaterial supported by an elastic beam. The inset shows the metamaterial's unit cell. (b) SEM images of the fabricated metamaterial (top) and the supporting elastic beam (bottom). (c) Measured reflectivity spectra of the sensor cavity for  $x$ - and  $y$ -polarized illumination without current or magnetic field.

metamaterial, resulting in weak or strong absorption,<sup>26</sup> respectively [Fig. 1(b)].

The metamaterial controls how the reflectivity of the sensor depends on the size of the cavity gap. This provides an opportunity to optimize responsivity, dynamic range, and linearity of the sensor by metamaterial design, allowing different sensing characteristics for different optical readout wavelengths and polarizations.<sup>27,28</sup> For example, low-loss non-resonant (high-loss resonant) metamaterial properties will yield narrow (wide) Fabry–Pérot resonances that result in large reflectivity changes over a small (large) range of displacements, i.e., high (low) responsivity over a small (large) dynamic range. Figure 2 shows the geometry and measured optical properties of a sensor that has been optimized for a quasi-linear sensor response in the near-infrared. The dependence of the reflectivity of a Fabry–Pérot cavity consisting of a metamaterial and a mirror on the cavity gap and the metamaterial's transmission and reflection coefficients has been derived in Ref. 27 in general. The resonant characteristics of such a cavity involving a metamaterial that is a split ring aperture array (as considered here) were studied in Ref. 28, and the resonances of such metamaterials as a function of split ring aperture geometry were investigated in Ref. 29.

For the design of the beam that supports the metamaterial, it is important to consider that the displacement of the beam is driven by the magnetic Lorentz force (desirable) but also by thermal actuation associated with resistive heating of the current-carrying beam (undesirable).<sup>30,31</sup> The magnetic displacement  $D_B$  is proportional to the Lorentz force and inversely proportional to the spring constant of the beam, which may be described by the Euler–Bernoulli beam theory;<sup>32,33</sup> therefore,

$$D_B \sim L^4 W^{-1} H^{-3} \mathbf{I} \times \mathbf{B}, \quad (1)$$

where  $W$  and  $H$  are the width and the thickness (height) of the beam. Considering bending of a bilayer due to resistive heating balanced by conductive cooling,<sup>34</sup> the thermal displacement  $D_T$  scales according to

$$D_T \sim L^4 W^{-2} H^{-3} I^2 \rho r \Delta\alpha, \quad (2)$$

where  $\rho$  and  $r$  are the effective electrical and thermal resistivities and  $\Delta\alpha$  is the difference between the thermal expansion coefficients of the layers. For the proof-of-principle demonstration of the sensor, we choose gold—due to its low electrical and thermal resistivity, and chemical stability—supported by silicon nitride due to easy availability in the form of membranes of nanoscale thickness. For a given choice of materials, it follows that the ratio of magnetic to thermal displacement is proportional to  $W/I$ , i.e., thermal effects will be suppressed in sensors that have a wide beam and operate at low current. That low-current operation is desirable can be easily understood by considering that electrical power dissipation, i.e., heating, is quadratically dependent on current, while the Lorentz force depends linearly on current, implying that the latter dominates at low currents. That wide beams are desirable can be understood by considering that magnetic displacement is inversely proportional to the beam's width (as its spring constant is proportional to  $W$ ), while thermal displacement is inversely proportional to the square of the width (due to both lower electrical and thermal resistance of wider beams). While wide beams and low currents suppress thermal displacement more strongly than magnetic actuation, the latter is also

suppressed. Therefore, it is important to choose the length and thickness of the beam in a way that achieves large beam displacements at small magnetic fields. As the beam displacement is proportional to  $L^4 H^{-3}$ , this implies that the beam should be as long and thin as reasonably achievable. Taking mechanical stability into account, we have chosen  $L = 250 \mu\text{m}$ ,  $W = 60 \mu\text{m}$ , and  $H = 100 \text{nm}$  [Fig. 2(a)].

### III. NANOMECHANICAL METAMATERIAL OPTICAL MAGNETIC FIELD SENSOR

The metamaterial and its supporting beam were fabricated by thermal evaporation of gold (50 nm) on a  $250 \times 250 \mu\text{m}^2$  silicon nitride membrane (50 nm), followed by focused ion beam milling of the beam actuator, metamaterial, and electrical insulation, which cuts through the gold film to create separate electrical terminals at either beam end [Fig. 2(b)]. Strips of the photoresist spacer were fabricated on a metallic mirror by standard photolithography to prevent physical contact between the mirror and metamaterial, and the cavity was assembled. Reflectivity spectra of the metamaterial microcavity [Fig. 2(c)] reveal a series of Fabry–Pérot resonances in the near-infrared part of the spectrum, with spectral positions that indicate a cavity gap of  $3.9 \mu\text{m}$ .

In the interest of a concise presentation, we will characterize the sensor with  $y$ -polarized incident light in this paper. Its properties for illumination with  $x$ -polarized light are qualitatively similar and shown in the [supplementary material](#) (Figs. S1 and S2).

To demonstrate optical magnetic field sensing, we studied the dependence of the sensor's reflectivity spectrum  $R(\lambda, I, B)$  on the electrical current  $I$  and magnetic field  $B$ . It is convenient to consider the relative reflectivity change,

$$\Delta(\lambda, I, B) = [R(\lambda, I, B) - R_0(\lambda)]/R_0(\lambda), \quad (3)$$

that results from the application of an electrical current along the beam actuator, where  $R_0(\lambda)$  is the reflectivity spectrum without the applied current. The spectral dependence of the sensor's reflectivity was measured with a microspectrophotometer. It depends strongly on both the current and magnetic field (Fig. 3). Without the magnetic field, currents of opposite sign yield the same reflectivity change [Fig. 3(a)], as expected according to Eq. (2) for the thermal displacement of the metamaterial that controls the cavity gap and thus the optical properties of the device. The reflectivity becomes dependent on the current direction in the presence of a magnetic field [Fig. 3(d)] due to competing thermal and magnetic displacement of the metamaterial according to Eqs. (1) and (2). Both contributions may be separated by exploiting that the thermal displacement does not depend on the current direction, but the magnetic displacement does. Therefore, the thermal reflectivity change is given by the average reflectivity change for opposite current directions,

$$\Delta_T(\lambda, I, B) = [\Delta(\lambda, I, B) + \Delta(\lambda, -I, B)]/2, \quad (4)$$

while the magnetic reflectivity change is given by the difference

$$\Delta_B(\lambda, I, B) = [\Delta(\lambda, I, B) - \Delta(\lambda, -I, B)]/2. \quad (5)$$

As should be expected, we observe the same thermal reflectivity change without [Fig. 3(b)] and with [Fig. 3(e)] the magnetic field. The observed thermal reflectivity change is proportional to the

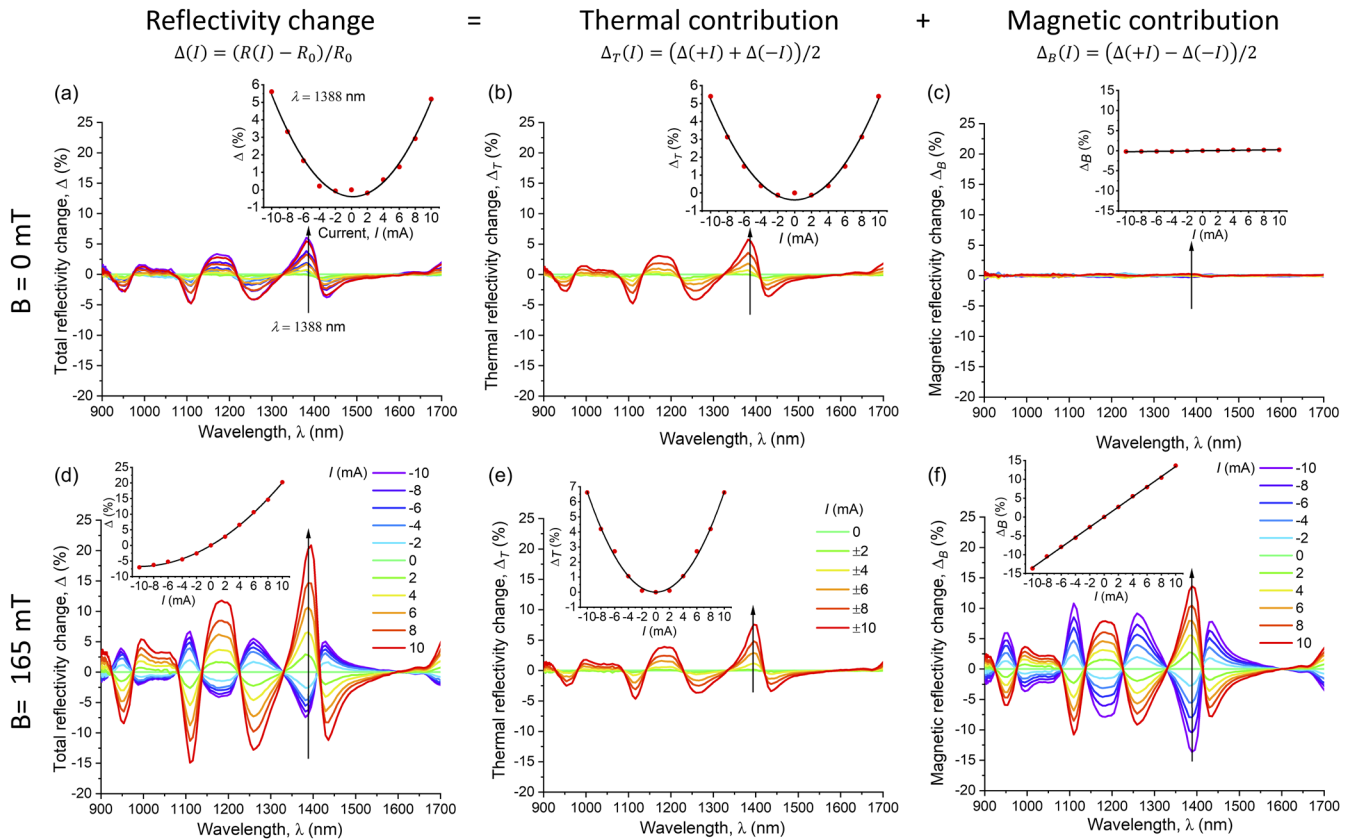


**FIG. 3.** Thermal and magnetic contributions to changes of the sensor's reflectivity. (a) and (d) Measured changes  $\Delta$  of the reflectivity spectrum due to the application of electrical current to the sensor are separated into (b) and (e) thermal contributions  $\Delta_T$  that do not depend on the current direction and (d) and (f) magnetic contributions  $\Delta_B$  that change sign for opposite current directions. Measurements (a)–(c) without and (d)–(f) with the magnetic field are presented and insets show results at the wavelength of 1388 nm. Results are shown for  $y$ -polarized illumination here and for  $x$ -polarized illumination in Fig. S1.

square of the applied current, i.e., it is proportional to the electrical power dissipated in the device [Eq. (2)]. With a resistance of 110  $\Omega$ , the sensor dissipates 11 mW when operated at 10 mA, resulting in thermal reflectivity changes of up to 6%. A magnetic reflectivity change is only observed in the presence of a magnetic field and depends linearly on the applied current [compare Figs. 3(c) and 3(f); see Eq. (1)]. At the same current and for 165 mT magnetic field, we observe magnetic reflectivity changes of up to 14%. While thermal and magnetic contributions to reflectivity changes of the sensor can be effectively separated using this approach, we note that the thermal contribution can also be suppressed relative to the magnetic one by operating the sensor at low currents. The largest reflectivity changes are observed at a wavelength of 1388 nm, which is slightly detuned from the sensor's 1410 nm resonance [Fig. 2(c)]. Near 1388 nm wavelength, the reflectivity spectrum is highly dispersive and thus a small shift of the resonance (due to thermal or magnetic actuation) yields a large reflectivity change. The characteristics of the Fabry–Pérot resonances are controlled by the gap and the optical properties of the metamaterial.<sup>28</sup>

Figure 4 illustrates the dependence of the magnetic reflectivity change  $\Delta_B$  on the magnetic field.  $\Delta_B$  is proportional to both the

current and magnetic field, as may be expected from metamaterial displacement driven by the magnetic Lorentz force. The observed magnetic reflectivity change per unit of current and magnetic field is  $\Delta_B/(IB) = 8000\%/(\text{AT})$  at 1388 nm wavelength [Fig. 4(b)]. Notably, the dynamic range of the sensor can be flexibly adjusted by changing the applied current, where lower current increases the dynamic range at the cost of reduced responsivity ( $\Delta_B/B$ ). Considering that the sensor is still in its linear regime (where  $\Delta_B \sim BI$ ) at 165 mT and 10 mA, it should allow measurements of at least 1.65 T ( $10\times$  larger) at 1 mA ( $10\times$  smaller). Indeed, while the Lorentz force  $F_L$ , magnetic displacement  $D_B$  [Eq. (1)], and magnetic reflectivity change  $\Delta_B$  should be the same for both cases, the unwanted thermal displacement  $D_T$  [Eq. (2)] and the associated thermal reflectivity change  $\Delta_T$  [Figs. 3(b) and 3(e)] should be  $100\times$  weaker at 1 mA.

In the static regime, a reliable detection of 0.1% reflectivity changes with a stable laser and photodetector translates to about 1 mT accuracy at 10 mA. This can be enhanced by resonant sensor operation with a sinusoidally oscillating current at the beam's fundamental mechanical resonance at  $f_0 = 234$  kHz and lock-in detection of the resulting reflectivity modulation (Fig. 5). The mechanical resonance provides resonantly enhanced beam displacement (and thus

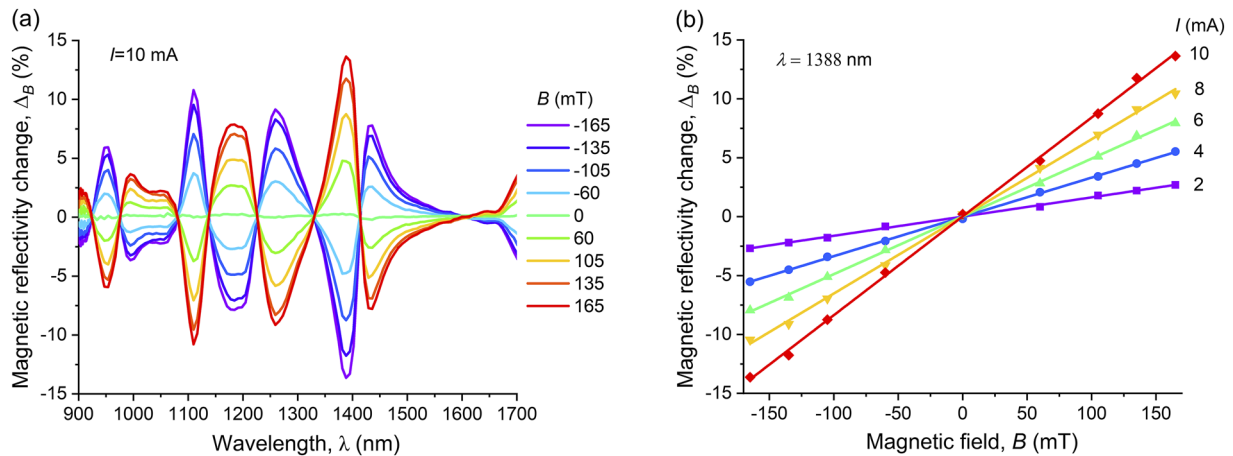


**FIG. 4.** Magnetic field sensing. (a) Measured spectral dependence of the magnetic reflectivity change  $\Delta_B$  for different magnetic fields at a current of 10 mA. (b) Magnetic reflectivity changes as a function of magnetic field for different currents at a wavelength of 1388 nm. Results are shown for y-polarized illumination here and for x-polarized illumination in Fig. S2.

reflectivity modulation), while detection locked to the oscillation frequency  $f$  improves the reflectivity modulation detection sensitivity. Such detection rejects any thermal effect, as the magnetic field yields resonantly enhanced reflectivity modulation at the detected frequency  $f$ , while resistive heating yields non-resonant modulation at  $2f$ . Indeed, thermal modulation is further suppressed by the high modulation frequency, which does not allow the metamaterial beam to cool in between heating cycles—the conductive cooling timescale of  $\sim 100 \mu\text{s}$  is around 50 times longer than the heating cycle of  $\sim 2 \mu\text{s}$  for resonant sensor operation. At the closest available laser wavelength of 1360 nm, we observe a 12 $\times$  resonant enhancement of the magnetic reflectivity modulation signal (and of the signal-to-noise ratio), with a reflectivity modulation noise level of 0.01% at an integration time of 10 ms. The same enhancement at a wavelength of 1388 nm implies  $\Delta_B/(IB) = 100000\%/(AT)$  for sensing at the mechanical resonance. Assuming the same noise for resonant sensor operation at 10 mA, the corresponding noise equivalent

magnetic field is  $1 \mu\text{T Hz}^{-0.5}$  at room temperature and atmospheric pressure, suggesting that sub-microtesla fields could be detected with integration times exceeding one second. A higher responsivity and/or a lower noise equivalent magnetic field may be expected from sensor operation at low pressure (higher resonant enhancement), low temperature (lower noise), and higher current (larger Lorentz force). Considering that the resonant displacement amplitude of a mechanical resonator with resonance frequency  $f_0$  and quality factor  $Q$  decays with a time constant of  $Q/(\pi f_0)$ , the mechanical response time of the sensor is about  $10 \mu\text{s}$ . We note a trade-off as a shorter, thicker beam (with higher  $f_0$ , where  $f_0 \sim HL^{-2}$ ) may be expected to shorten the mechanical response time at the cost of reduced responsivity (smaller beam displacement), and low pressure (higher  $Q$ ) would increase the responsivity at the cost of a slower response. While the spatial resolution of our sensor is given by the beam width of  $60 \mu\text{m}$ , we note that recent experimental demonstrations of individual electrical addressing<sup>35</sup> and optical readout<sup>36,37</sup> of metamaterial beams with sub-micron spacing indicate that such sensors can be realized as arrays for magnetic field sensing with few micron (possibly even sub-micron) spatial resolution.

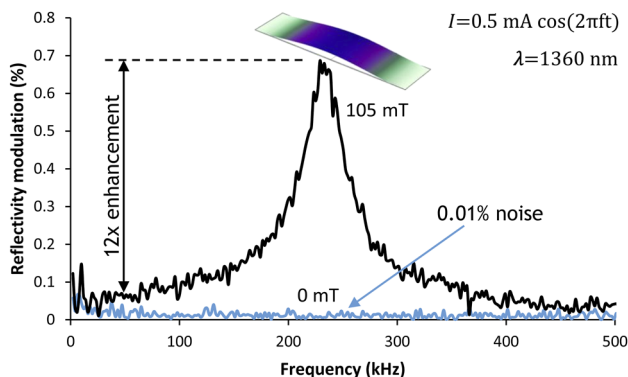


**FIG. 5.** Resonant enhancement of responsivity and signal-to-noise ratio. Measured reflectivity modulation at frequency  $f$  when driving the sensor with a current of  $I = 0.5 \text{ mA} \cos(2\pi ft)$  for magnetic fields of 0 and 105 mT. The inset shows the beam's resonant mechanical mode.

#### IV. CONCLUSIONS

In summary, we have demonstrated that Lorentz-force-actuated metamaterial microcavities enable optical magnetic field sensing with non-contact readout. Combining nanomechanics, photonics, and metamaterials, we realized an optical magnetic field sensor of microscale size as well as spatial resolution and demonstrated the sensing principle experimentally. Our measurements indicate that the proof-of-concept metamaterial magnetometer can provide  $10 \mu\text{s}$  time resolution and a sub-microtesla to tesla dynamic range.

#### SUPPLEMENTARY MATERIAL

See the [supplementary material](#) for the characterization of the optical magnetic field sensor with x-polarized light.

## ACKNOWLEDGMENTS

This work was supported by the Office of Naval Research (Grant No. N62909-18-1-2026), the UK's Engineering and Physical Sciences Research Council (Grant Nos. EP/M009122/1 and EP/T02643X/1), the Singapore Ministry of Education [Grant No. MOE2016-T3-1-006 (S)], and the Basic Scientific Research of Heilongjiang University (Grant No. 2020-KYYWF-0997).

## AUTHOR DECLARATIONS

### Conflict of Interest

The authors have no conflicts to disclose.

## DATA AVAILABILITY

The data that support the findings of this study are openly available in the University of Southampton ePrints research repository at <https://doi.org/10.5258/SOTON/D2057>.<sup>38</sup>

## REFERENCES

- 1 P. Galland and A. Pazur, "Magnetoreception in plants," *J. Plant Res.* **118**, 371–389 (2005).
- 2 W. W. Roswitha Wiltschko, "Magnetoreception," *BioEssays* **28**, 157–168 (2006).
- 3 W. Lowrie, *Fundamentals of Geophysics* (Cambridge University Press, London, 2007).
- 4 S. Tumanski, *Handbook of Magnetic Measurements* (CRC Press, 2016).
- 5 C. V. Nelson, "Metal detection and classification technologies," Johns Hopkins APL Tech. Dig. **25**, 62–67 (2004).
- 6 H. Hu, H. Zhong, C. Chen, and Q. Chen, "Magnetically responsive photonic watermarks on banknotes," *J. Mater. Chem. C* **2**, 3695–3702 (2014).
- 7 Y. Ouyang, J. He, J. Hu, and S. X. Wang, "A current sensor based on the giant magnetoresistance effect: Design and potential smart grid applications," *Sensors* **12**, 15520–15541 (2012).
- 8 P. Schmidt, D. Clark, K. Leslie, M. Bick, D. Tilbrook, and C. Foley, "Getmag—A SQUID magnetic tensor gradiometer for mineral and oil exploration," *Explor. Geophys.* **35**, 297–305 (2004).
- 9 M. Aguilar, G. Alberti, B. Alpat, A. Alvino, G. Ambrosi, K. Andeen, H. Anderhub, L. Arruda, P. Azzarello, and A. Bachlechner, "First result from the alpha magnetic spectrometer on the international space station: Precision measurement of the positron fraction in primary cosmic rays of 0.5–350 GeV," *Phys. Rev. Lett.* **110**, 141102 (2013).
- 10 J. E. Lenz, "A review of magnetic sensors," *Proc. IEEE* **78**, 973–989 (1990).
- 11 D. Robbes, "Highly sensitive magnetometers—A review," *Sens. Actuators, A* **129**, 86–93 (2006).
- 12 F. Keplinger, S. Kvasnica, A. Jachimowicz, F. Kohl, J. Steurer, and H. Hauser, "Lorentz force based magnetic field sensor with optical readout," *Sens. Actuators, A* **110**, 112–118 (2004).
- 13 R. Mhaskar, S. Knappe, and J. Kitching, "A low-power, high-sensitivity micromachined optical magnetometer," *Appl. Phys. Lett.* **101**, 241105 (2012).
- 14 L. Sun, S. Jiang, and J. R. Marcianite, "All-fiber optical magnetic-field sensor based on Faraday rotation in highly terbium-doped fiber," *Opt. Express* **18**, 5407–5412 (2010).
- 15 N. Itoh, H. Minemoto, D. Ishiko, and S. Ishizuka, "Small optical magnetic-field sensor that uses rare-earth iron garnet films based on the Faraday effect," *Appl. Opt.* **38**, 2047–2052 (1999).
- 16 Y. Chen, Q. Han, T. Liu, X. Lan, and H. Xiao, "Optical fiber magnetic field sensor based on single-mode-multimode-single-mode structure and magnetic fluid," *Opt. Lett.* **38**, 3999–4001 (2013).
- 17 Y. Zhao, R. Lv, D. Wang, and Q. Wang, "Fiber optic Fabry-Perot magnetic field sensor with temperature compensation using a fiber Bragg grating," *IEEE Trans. Instrum. Meas.* **63**, 2210–2214 (2014).
- 18 Y. Zhao, R. Lv, Y. Ying, and Q. Wang, "Hollow-core photonic crystal fiber Fabry-Perot sensor for magnetic field measurement based on magnetic fluid," *Opt. Laser Technol.* **44**, 899–902 (2012).
- 19 D. L. Sage, K. Arai, D. R. Glenn, S. J. DeVience, L. M. Pham, L. Rahn-Lee, M. D. Lukin, A. Yacoby, A. Komeili, and R. L. Walsworth, "Optical magnetic imaging of living cells," *Nature* **496**, 486–489 (2013).
- 20 J. F. Barry, M. J. Turner, J. M. Schloss, D. R. Glenn, Y. Song, M. D. Lukin, H. Park, and R. L. Walsworth, "Optical magnetic detection of single-neuron action potentials using quantum defects in diamond," *Proc. Natl. Acad. Sci. U. S. A.* **113**, 14133–14138 (2016).
- 21 D. Budker and M. Romalis, "Optical magnetometry," *Nat. Phys.* **3**, 227–234 (2007).
- 22 D. K. Wickenden, J. L. Champion, R. Osiander, R. B. Givens, J. L. Lamb, J. A. Miragliotta, D. A. Oursler, and T. J. Kistenmacher, "Micromachined polysilicon resonating xylophone bar magnetometer," *Acta Astronaut.* **52**, 421–425 (2003).
- 23 B. Park, M. Li, S. Liyanage, and C. Shafai, "Lorentz force based resonant MEMS magnetic-field sensor with optical readout," *Sens. Actuators, A* **241**, 12–18 (2016).
- 24 D. J. Vasquez and J. W. Judy, "Optically-interrogated zero-power MEMS magnetometer," *J. Microelectromech. Syst.* **16**, 336–343 (2007).
- 25 N. I. Zheludev and E. Plum, "Reconfigurable nanomechanical photonic metamaterials," *Nat. Nanotechnol.* **11**, 16–22 (2016).
- 26 E. Plum, K. F. MacDonald, X. Fang, D. Faccio, and N. I. Zheludev, "Controlling the optical response of 2D matter in standing waves," *ACS Photonics* **4**, 3000–3011 (2017).
- 27 P. Cencillo-Abad, N. I. Zheludev, and E. Plum, "Metadevice for intensity modulation with sub-wavelength spatial resolution," *Sci. Rep.* **6**, 37109 (2016).
- 28 P. Cencillo-Abad, J. Y. Ou, E. Plum, and N. I. Zheludev, "Electro-mechanical light modulator based on controlling the interaction of light with a metasurface," *Sci. Rep.* **7**, 5405 (2017).
- 29 E. Plum, K. Tanaka, W. T. Chen, V. A. Fedotov, D. P. Tsai, and N. I. Zheludev, "A combinatorial approach to metamaterials discovery," *J. Opt.* **13**, 055102 (2011).
- 30 J. Valente, J. Y. Ou, E. Plum, I. J. Youngs, and N. I. Zheludev, "A magneto-electro-optical effect in a plasmonic nanowire material," *Nat. Commun.* **6**, 7021 (2015).
- 31 J. Valente, J. Y. Ou, E. Plum, I. J. Youngs, and N. I. Zheludev, "Reconfiguring photonic metamaterials with currents and magnetic fields," *Appl. Phys. Lett.* **106**, 111905 (2015).
- 32 S. Schmid, L. G. Villanueva, and M. L. Rourke, *Fundamentals of Nanomechanical Resonators* (Springer, 2016).
- 33 J. M. Gere and S. P. Timoshenko, *Mechanics of Materials* (PWS, 1997).
- 34 S. Prasanna and S. M. J. Spearing, "Materials selection and design of micro-electrothermal bimaterial actuators," *J. Microelectromech. Syst.* **16**, 248–259 (2007).
- 35 P. Cencillo-Abad, J. Y. Ou, E. Plum, J. Valente, and N. I. Zheludev, "Random access actuation of nanowire grid metamaterial," *Nanotechnology* **27**, 485206 (2016).
- 36 J. Y. Ou, E. Plum, and N. I. Zheludev, "Optical addressing of nanomechanical metamaterials with subwavelength resolution," *Appl. Phys. Lett.* **113**, 081104 (2018).
- 37 D. Papas, J. Y. Ou, E. Plum, and N. I. Zheludev, "Optomechanical metamaterial nanobolometer," *APL Photonics* **6**, 126110 (2021).
- 38 G. Lan, J. Y. Ou, D. Papas, N. I. Zheludev, and E. Plum (2021). "Dataset for non-contact optical magnetic field sensor based on metamaterial nanomechanics," University of Southampton ePrints research repository. <https://doi.org/10.5258/SOTON/D2057>